Mapping the Material Microstructure of Safety Critical Components Using Ultrasonic Phased Arrays

Katherine M. M. Tant
and Anthony J. Mulholland
Department of Mathematics and Statistics
University of Strathclyde
Glasgow, U.K.
Email: katy.tant@strath.ac.uk

Erica Galetti
and Andrew Curtis
School of Geosciences
University of Edinburgh
Edinburgh, U.K.

Anthony Gachagan
Centre of Ultrasonic Engineering
University of Strathclyde
Glasgow, U.K.

***Abstract*—Traditional imaging algorithms within the ultrasonic NDE community typically assume that the material being inspected is homogeneous. Obviously, when the medium is of a heterogeneous or anisotropic nature this assumption can contribute to the poor detection, sizing and characterisation of defects. Knowledge of the internal structure and properties of the material would allow corrective measures to be taken. The work presented here endeavours to reconstruct coarsened maps of the locally anisotropic grain structure of industrially representative samples from ultrasonic phased array data. This is achieved via application of the reversible-jump Markov Chain Monte Carlo (rj-MCMC) method: an ensemble approach within a Bayesian framework. The resulting maps are used in conjunction with the total focussing method and the reconstructed flaws are used as a quantitative measure of the success of this methodology. Using full matrix capture data arising from a finite element simulation of a phased array inspection of an austenitic weld, a 71% improvement in flaw location and an 11dB improvement in SNR is achieved using no *a priori* knowledge of the material's internal structure.**

I. Introduction

Ultrasonic non-destructive evaluation relies on the transmission and reception of mechanical waves to image the interior of solid objects without compromising their structural integrity. It is particularly important for the testing of key components within safety critical industries such as nuclear, oil and gas, power, and aerospace, where failure to detect structural weaknesses is potentially catastrophic. Ultrasonic phased arrays (which are capable of simultaneously transmitting and receiving ultrasound signals across multiple piezoelectric elements) provide the possibility of performing fast inspections with ultrasonic beams at various angles and focal lengths, giving rise to a richer set of data. The N^2 A-scans arising from each transmit/receive pair of elements can be stored in a 3D matrix usually termed the Full Matrix Capture (FMC) [1] (with dimensions $N \times N \times T$, where T is determined by the length of the A-scan). These FMC datasets can be processed to create images of the internal structure of the object, thus highlighting any flaws. However, traditional imaging algorithms can struggle to accurately reconstruct defects within the component when the material exhibits inhomogeneous and/or anisotropic behaviour. Due to the spatial variation of material properties, the ultrasonic wave paths are distorted and their expected arrival times, on which classical imaging algorithms are based, are no longer accurate.

One example of this behaviour occurs in austenitic welds where, due to the heating process during their formation, a polycrystalline structure develops and large misorientated grains cause waves to scatter and bend. When traditional imaging algorithms (which assume a homogeneous medium with constant wave speed [1]) are applied to these datasets, flaws are typically mislocated and poorly characterised. To overcome this issue, knowledge of the material map can be used in conjunction with imaging algorithms to correct for deviations in the velocity of the wave as it travels through the sample [2]. There exist several strategies for obtaining these maps. Very accurate, high resolution reconstructions of the material microstructure can be extracted via experimental means such as electron backscatter diffraction (EBSD) [3] and spatially resolved acoustic spectroscopy (SRAS) [4]. However, these techniques require cross sections of the material to be sliced and polished and thus contradict the basic principles of NDE. Another means to obtaining a material map is via forward modelling. MINA (Modeling of anIsotropy based on Notebook of Arcwelding) uses information from the welding procedure to predict the final geometry of the weld structure [5]. However, it is obviously restricted to the mapping of welds and requires *a priori* knowledge of the welding process which may not always be available when examining historic welds.

Reconstruction of the material geometry can alternatively be approached as an inverse problem, where properties of the material can be inferred from its ultrasonic phased array inspection. In [6], [7], the thickness of plate-like structures is mapped using guided wave tomography. A tomographic approach to reconstructing the internal crystalline structure of a weld has previously been employed in [2], where an initial

estimate of the weld microstructure was taken from a model and the ultrasonic wave propagation through the weld was simulated using Dijkstra's shortest path algorithm. The weld parameters were then varied and the error between the experimental data and modelled data was minimised. Once the error converged, a weld map was generated and used in conjunction with the total focussing method (TFM) [1] to produce more accurate images of a flaw. In this paper, a similar approach is taken but with some key differences. Here, the reversible jump Markov Chain Monte Carlo (rj-MCMC) method [8], an ensemble inference approach within a Bayesian framework, is used. One benefit of the rj-MCMC is that it treats the model dimension as an unknown: the method is transdimensional. Thus, instead of being restricted to a high dimensional rigid square mesh as used in [2], the parametrisation of the internal geometry is adaptive and will naturally adapt to the lowest dimensional space suitable to best model the distinct regions present in the sample under inspection. However, as we study moments of the *ensemble* solution (specifically the mean of the posterior distribution of solutions to our inverse problem) this discrete partitioning is replaced by a continuous map of the spatial domain, thus removing any limits on its resolution. Additionally, no assumptions are required on the internal structure of the sample under inspection; the initial model arbitrarily assigns a constant dominant orientation to the entire domain. The only prior information required is that which can be measured directly: the sample's dimensions, the location of the transmitting and receiving elements and the material's slowness curve (derived from the known elastic constants). The method has already been used successfully within the seismology community to chart the velocity field of the Earth's surface [9], [10]. In this work, as we are primarily concerned with polycrystalline structures where the material properties are constant but the wave speed is dependent on the wave direction and grain orientations, a single map of the velocity field cannot represent the complexity of the material. Instead, a map of regions with dominant orientations is reconstructed, mirroring the polycrystalline properties of the sample. This map is then used in conjunction with the TFM to correct for discrepancies in the expected arrival times caused by the anisotropic nature of the material.

II. Method

A. Material Parametrisation

To minimise the degrees of freedom within the inversion, it is assumed that regions of contiguous crystallites with similar orientations can be grouped together and assigned an average orientation, producing a coarsened representation of the material microstructure. These regions will be referred to as *grains* throughout this paper and will be represented by *cells* in the geometrical parametrisation of the microstructure. As the polycrystalline materials in which we are primarily interested in have an irregular geometry, Voronoi diagrams will be used to describe them mathematically [11], [12]. This partitioning is dictated by a discrete set of seeds (x_i, y_i) for $i = 1, ..., n$, where n is the number of regions, creating $2n$ degrees of freedom. To parameterise the polycrystalline material, a third parameter is assigned to each cell: its orientation ϕ_i. This orientation dictates the speed at which a wave passes through that grain and allows the effects of anisotropy to be studied. Thus we have a parametrisation with $3M$ unknowns (where M, the number of cells, is itself an unknown), and N^2 equations, describing the known time of arrival between every transmit/receive pair of elements.

B. The Reversible-Jump Markov Chain Monte Carlo Algorithm

The reversible-jump Markov Chain Monte Carlo (rj-MCMC) method produces a posterior distribution for transdimensional spaces. It is an ensemble approach based in a Bayesian framework and thus requires that all information is written in terms of probabilities. The posterior probability density function is given by Bayes' rule

$$p(\mathbf{m}|\mathbf{d}_{obs}) \propto p(\mathbf{d}_{obs}|\mathbf{m})p(\mathbf{m}) \tag{1}$$

where $p(\mathbf{m})$ is the *a priori* probability density function of the model $\mathbf{m}$ and $p(\mathbf{d}_{obs}|\mathbf{m})$ is the likelihood that the observed data $\mathbf{d}_{obs}$ arises from that model. The distance between the observed data and the model is measured using the least squares misfit function

$$\text{misfit} = \left\| \frac{f(\mathbf{m}) - f(\mathbf{d}_{obs})}{\sigma_d} \right\|^2 \tag{2}$$

where σ_d^2 is the variance of the data noise [13] and the function f represents the estimated first time of arrivals for each transmit/receive pair of array elements from the dataset on which it is acting. This is equivalent to maximising the probability for a Gaussian likelihood function and so

$$p(\mathbf{d}_{obs}|\mathbf{m}) \propto \exp\left(\frac{-\text{misfit}}{2}\right). \tag{3}$$

A priori information is included via the $\mathbf{p}(\mathbf{m})$ term and is kept to a minimum by drawing the model parameters from uninformative uniform distributions, and only using information which is directly measurable: the exterior dimensions of the imaging domain and the locations of the transmitters and receivers.

To generate a reliable estimate of the posterior distribution, the model must be evaluated iteratively throughout the model space. An initial parametrisation of the material microstructure $\mathbf{m}$ is constructed using a Voronoi diagram. An arbitrary number of cells is taken and they are all assigned the same value of ϕ_i. A straight ray between each pair of transmit/receive elements is modelled (to minimise the computational expense, the effects of raybending are ignored in this paper). Slowness curves [14] are used to dictate the velocity at which the ray travels. This is dependent on the direction of the wave θ and the angle ϕ_i of each region the ray passes through. Coupled with the known distances through each distinct cell lying between the transmit and receive elements, a first time of arrival for each pair is predicted to obtain the Time-of-Flight matrix (ToF). The distance between the modelled ToF matrix

and observed ToF matrix is then calculated using equation (2) and the posterior $p(\mathbf{m}|\mathbf{d}_{obs})$ for the initial model is thus evaluated. The geometry is then perturbed to create a new model $\mathbf{m}'$. This can be done in one of five ways: cell birth, cell death, cell move, cell orientation change or system noise change [13]. Once a perturbation has been made, the posterior $p(\mathbf{m}'|\mathbf{d}_{obs})$ is calculated. The perturbation is then accepted or rejected subject to the Metropolis-Hastings criteria

$$p(\text{accept}) = \min\left(1, \frac{p(\mathbf{m}'|\mathbf{d}_{obs})}{p(\mathbf{m}|\mathbf{d}_{obs})}\right). \tag{4}$$

Once accepted, the model $\mathbf{m}'$ replaces the model $\mathbf{m}$ and the process begins again. If $\mathbf{m}'$ is rejected, the model is discarded and the original model $\mathbf{m}$ is perturbed again.

C. Sampling the Posterior Distribution

The above process is repeated iteratively and, due to the nature of the Markov chain and its *memoryless* property [15], each perturbation is independent of all previous model perturbations. After the *burn in* period, the Markov chain should converge and exhibit stationarity: this is the posterior distribution of solutions to the inverse problem. By excluding the burn in period, any bias towards the initial model is discounted. The chain is then sampled at an interval of r, where r is the number of steps required before we can expect to obtain a model that is considered independent of the last. In deterministic optimisation schemes, the model with the smallest misfit (the global minimum) would typically be taken as the solution. However, within the Bayesian framework, we are encouraged to consider the posterior distribution as a whole and so instead of considering a single model, various moments of the distribution are analysed. To produce the mean image of the material map we project the sampled partition models into the spatial domain and average. Given the large number of samples, when the Voronoi tessellations are stacked, the partitions overlap and the resulting spatial regional orientation map is effectively a continuous function of the plane. This framework allows the study of the variance over the domain which can be exploited for uncertainty quantification studies and probability of detection work.

D. The Observed Data

For this paper, to minimise the uncertainty in the extraction of the first time of arrival data, a through-transmission set up has been selected for the simulated inspection, where the transmitting and receiving arrays are placed directly opposite each other on each side of the sample. Thus, the time of flight matrix can be constructed by taking the first point in time at which the amplitude of the signal reaches a pre-determined threshold (chosen as 1.5μV here) for each pair of transmit/receive elements.

E. Simulation

1) Synthetic Geometry: A simplified model was examined first to allow visual analysis of the algorithm's success. A finite element simulation of a through-transmission phased array inspection of a sample constructed from four distinct *grains* (as shown in Figure 1a) was run (recall that regions of contiguous crystallites with similar orientations are grouped together and assigned an average orientation and referred to as *grains*). Each grain was assigned the same material properties but the upper right and bottom left grains (in yellow) were assigned a 20° orientation and the remaining two grains were assigned a 0° orientation. The rj-MCMC algorithm was run for 50,000 samples and assumed to be stationary after around 1000 samples. These first 1000 samples were discarded (the *burn in* period) and the remaining models were sampled at an interval of 100; it is these sampled models from which our statistics are drawn. Figure 1b depicts an arbitrary sample drawn from the posterior distribution and a resemblance to the known geometry is indeed apparent. The distance between the two can be quantified in terms of the total error difference between the image matrices averaged over the number of pixels. This measure gives an average error of 4.3° per pixel between the sample shown in Figure 1b and the known geometry. This compares favourably to the difference between the initial map (where each cell was assigned an orientation of 10°) and the known geometry, where the error present at each pixel was 10°. Figure 1c depicts the mean of the posterior distribution and is the map which we take to be our solution to the inverse problem. The distance between it and the known geometry is further improved with an average error of 3.4°. The standard deviation of each pixel over the posterior distribution is plotted in Figure 1d. Note that where the mean map in image 1c diverges from the known geometry, primarily at the boundaries between differently orientated regions, a higher standard deviation is exhibited, from which we can infer that these areas are a less reliable representation of the actual material.

2) Simulated Inspection of a Weld: To test our method on more industrially relevant data, an ultrasonic phased array inspection of an austenitic weld was simulated in the software package PZFlex [16]. The weld microstructure was taken from experimental Electron Backscatter Diffraction (EBSD) measurements [3], [17] to allow the effects of the anisotropic polycrystalline structure of the weld on the wave's passage to be studied. Two simulations were run: the first was a through-transmission inspection of the weld material and the second was a one sided pulse-echo inspection where a 4mm diameter void was embedded in the centre of the weld geometry (see [18] for an in depth description of the simulation and the parameters used). The first time of arrivals between each pair of elements were extracted from the dataset arising from the through-transmission simulation in the same manner as discussed in Section II-D, and the rj-MCMC method was then applied. Here, the success of this map is measured via its use in conjunction with the TFM algorithm [1] in application to the one-sided inspection dataset which includes the void defect. The flaw reconstruction displayed in Figure 2a arises from application of the TFM when the material is assumed to be isotropic and homogeneous. Application of the rj-MCMC algorithm resulted in the reconstruction of an anisotropic map

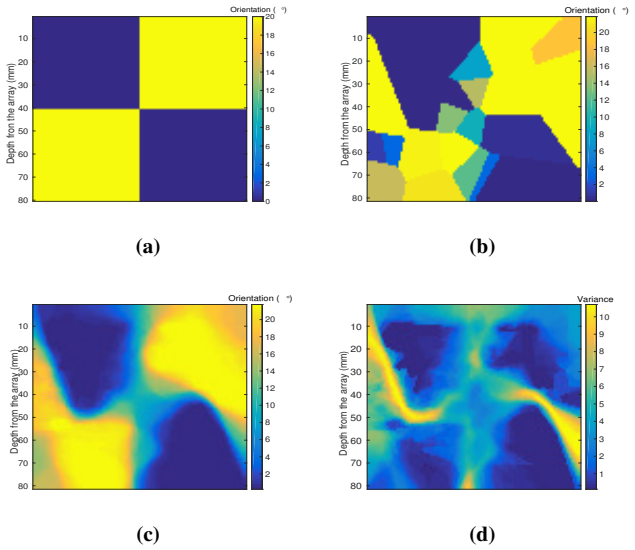

Fig. 1: Maps of a synthetic material with locally anisotropic regions: (a) the known geometry of the material as simulated within the PZFlex environment, (b) a Voronoi diagram taken from the stationary posterior distribution, (c) the ensemble average map and (d) the map of the standard deviation.

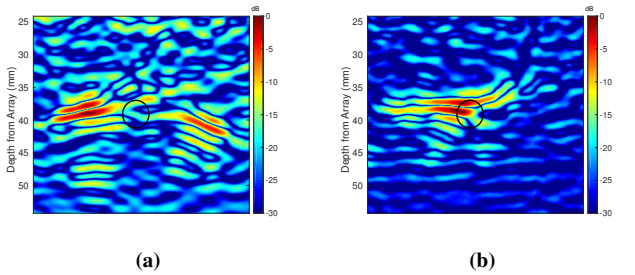

Fig. 2: TFM reconstructions of a 4mm void embedded in an austenitic weld where (a) a constant velocity assumption is made and (b) the rj-MCMC map is used in conjunction with the TFM. The hollow disc represents the known location and size of the defect.

of the weld which has been used to provide correction to the TFM imaging algorithm, as shown in Figure 2b. In image 2a, two separate high amplitude regions can be observed. Taking the stronger reflection on the left to be the flaw we have an SNR measurement of 15dB and an error in placement of 8.4mm. Image 2b exhibits an improved SNR of 26dB and a defect misplacement of only 2.4mm.

III. Conclusion

A new method for inverting ultrasonic phased array inspection data to reconstruct maps of the locally anisotropic grain structure of polycrystalline materials has been described. The material microstructure is parameterised using Voronoi diagrams and the final map is obtained by taking the mean of the posterior distribution of solutions to the inverse problem generated using the reversible-jump Markov Chain Monte Carlo method. Application to data arising from the finite element simulation of an ultrasonic phased array inspection of a synthetic material and an austenitic weld demonstrated the potential of the technique. In the case of the austenitic weld geometry, the success of the map was measured using the TFM reconstruction of a 4mm diameter void as a proxy. It was shown that an 11dB improvement in SNR could be obtained and the error in the reconstructed flaw's location improved by 6mm when the map of locally anisotropic regions was accounted for.

Acknowledgement

The core funding for this work has been provided by the UK Research Centre for NDE (EPSRC Grant EP/L022125/1).

References

[1] C. Holmes and B. W. Drinkwater and P. D. Wilcox. "Post processing of the full matrix of ultrasonic transmit receive array data for non destructive evaluation." NDT & E Int, vol. 38, no. 8, pp. 701-711, 2005.

[2] J. Zhang and A. Hunter and B. W. Drinkwater and P. D. Wilcox. "Monte Carlo inversion of ultrasonic array data to map anisotropic weld properties." IEEE TUFFC, vol. 59, no. 11, pp. 2487-2497, 2012.

[3] C. Nageswaran and C. Carpentier and Y. Y. Tse. "Microstructural quantification, modelling and array ultrasonics to improve the inspection of austenitic welds." Insight-Non-Destructive Testing and Condition Monitoring, vol. 51, no. 12, pp. 660-666, 2009.

[4] S. D. Sharples and M. Clark and M. G. Somekh. "Spatially resolved acoustic spectroscopy for fast noncontact imaging of material microstructure." Optics Express, vol. 14, no. 22, pp. 10435-10440, 2006.

[5] J. Moysan and A. Apfel and G. Corneloup and B. Chassignole. "Modelling the grain orientation of austenitic stainless steel multipass welds to improve ultrasonic assessment of structural integrity." International Journal of Pressure Vessels and Piping, vol. 80, no. 2, pp. 77-85, 2003.

[6] P. B. Nagy and F. Simonetti and G. Instanes. "Corrosion and erosion monitoring in plates and pipes using constant group velocity Lamb wave inspection." Ultrasonics, vol. 54, no. 7, pp. 1832–1841, 2014.

[7] P. Huthwaite and F. Simonetti. "High-resolution guided wave tomography." Wave Motion, vol. 50, no. 5, pp. 979–993, 2013.

[8] P. J. Green. "Reversible jump Markov chain Monte Carlo computation and Bayesian model determination." Biometrika, vol. 82, no. 4, pp. 711-732, 1995.

[9] T. Bodin and M. Sambridge and K. Gallagher. "A self-parametrizing partition model approach to tomographic inverse problems." Inverse Problems, vol. 25, no. 5, pp. 055009, 2009.

[10] E. Galetti and A. Curtis and G. A. Meles and B. Baptie. "Uncertainty loops in travel-time tomography from nonlinear wave physics." Physical review letters, vol. 114, no. 14, pp. 148501, 2015.

[11] A. Okabe and B. Boots and K. Sugihara and S. N. Chiu. Spatial Tessellations: Concepts and Applications of Voronoi Diagrams. John Wiley & Sons, 2009.

[12] A. Van Pamel and C. R. Brett and P. Huthwaite and M. J. S. Lowe. "Finite element modelling of elastic wave scattering within a polycrystalline material in two and three dimensions." JASA, vol. 138, pp. 2326-2336, 2015.

[13] T. Bodin and M. Sambridge and N. Rawlinson and P. Arroucau. "Transdimensional tomography with unknown data noise." Geophysical Journal International, vol. 189, no. 3, pp. 1536-1556, 2012.

[14] J. D. Achenbach. Wave Propagation in Elastic Solids. North Holland, 1973

[15] R. C. Aster, B. Borchers and C. H. Thurber. Parameter Estimation and Inverse Problems. 2nd ed. Elsevier Inc. 2013.

[16] PZFlex, Thornton Tomasetti Defence Ltd. 6th Floor South, 39 St Vincent Place, Glasgow, Scotland, G1 2ER, United Kingdom

[17] G. Harvey and A. Tweedie and C. Carpentier and P. Reynolds. "Finite element analysis of ultrasonic phased array inspections on anisotropic welds." AIP Conf. Proc., San Diego, California, pp. 827-834, July 2010.

[18] L. J. Cunningham, A. J. Mulholland, K. M. M. Tant,A. Gachagan, G. Harvey and C. Bird. "The detection of flaws in austenitic welds using the decomposition of the time-reversal operator." Proc. R. Soc. A, vol. 472, no. 2188, pp. 20150500, 2016.